COMMUNICATION

Check for updates

Material-dependent performance of fuel-free, light-activated, self-propelling colloids†

Andrew Leeth Holterhoff,[a] Victoria Girgis[a] and John G. Gibbs ★[ab]

Self-propelling, light-activated colloidal particles can be actuated in water alone. Here we study the effect of adding different amounts of a gold/palladium alloy to titanium dioxide-based, active colloids. We observe a correlation between alloy-thickness and the average speed of the particles, and we discover an intermediate thickness leads to the highest activity for this system. We argue that a non-continuous thin-film of the co-catalyst improves the efficiency of water-splitting at the surface of the particles, and in-turn, the performance of "fuel-free" self-propulsion.

Significant strides have recently been made in the field of self-propelled active colloids.[1–5] The community has been consistent in developing ever more sophisticated "active" particle schemes as a means of illuminating fundamental understanding,[6–9] and for targeting advanced micro- and nano-scale applications.[10,11] A promising design involves constructing active colloids from photocatalytic materials.[12–14] Advantages include on-command control over the activity—and other effects[15] such as non-equilibrium self-assembly—by simply changing the intensity of the excitation light, as well as the ability to induce self-propulsion in water alone, i.e. without the need for toxic chemicals.

Previous investigations have demonstrated the latter, sometimes described as "fuel-free" self-propulsion,[16] and from the literature, it is apparent that only certain morphologies and materials combinations allow for this effect to be observed. These designs typically require the particles to be constructed from two different materials that are in direct physical contact—forming a heterojunction[17]—which promotes efficient water splitting and indirectly, self-propulsion. It appears that no previous reports have systematically investigated the relationship between materials properties and the efficiency of fuel-free propulsion, but this knowledge should allow for the next

generation of advanced active matter systems. Here, we study light-activated, metal-semiconductor colloids that undergo self-propulsion in water alone, and we systematically alter the ratio of the two materials in order to determine which gives the highest activity. This study suggests fine-tuning materials properties is a practical method for optimizing the performance of fuel-free, light-activated particles that can be easily extended to other active particle morphologies beyond those reported herein.

Photocatalyst-based colloids may become self-propelling due to photocatalytic water splitting,[18]

$$2H_2O \rightarrow 2H_2 + O_2, \qquad (1)$$
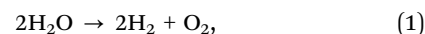
taking place on the surface of the particles. As an endothermic process, energy is required for this reaction to proceed, and photocatalysts can convert light into energy available for this task.[18] Take anatase titanium dioxide (TiO_2) as an example: with a band-gap energy $E_g \sim 3.2$ eV, a photon of ultraviolet (UV)-light may result in the formation of an electron e^- and a hole h^+, which can migrate to the surface of the photocatalyst and enable the water splitting process.[19] To the best of our knowledge, there have been no reports of active colloids constructed from a single catalytic material that self-propel in water alone. As a couple of examples, colloids of pure TiO_2[20] or Janus particles made from silica (SiO_2) and TiO_2,[15] appear to require hydrogen peroxide (H_2O_2)—in addition to UV-light—for propulsion to be observed. However, TiO_2-based particles can be propelled in only water when another catalytic material—a co-catalyst—is in direct contact with the titania, as has been demonstrated with metals[16,17] and semiconductors.[21] Such heterojunction-based materials are well documented as a medium for improving the efficiency of water-splitting for the production of hydrogen fuel,[22] and this same improved efficiency is likewise expected to allow for fuel-free self-propulsion in active colloids. However, the efficiency is also a function of the manner in which the two materials are in contact as well as the relative amounts, which is the focus of the present investigation.

The underlying structure of the active colloids herein are Janus particles that consist of microspheres (SiO_2) and a slightly

[a] Department of Applied Physics and Materials Science, Northern Arizona University, Flagstaff, AZ 86011, USA. E-mail: john.gibbs@nau.edu; Tel: +928 523 1916

[b] Center for Materials Interfaces in Research and Applications, Northern Arizona University, Flagstaff, AZ 86011, USA
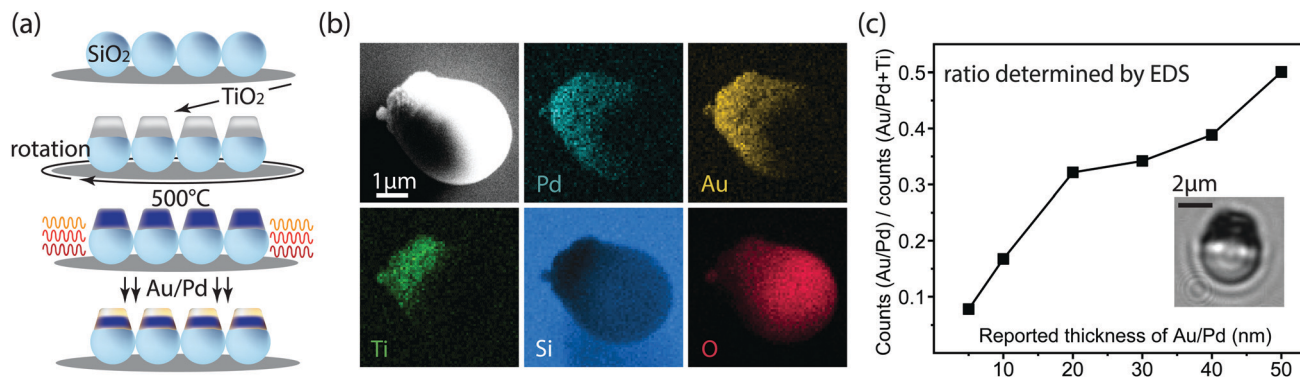
Fig. 1 (a) The fabrication process moving from top of schematic to bottom: a monolayer of ∼3.2 µm SiO$_2$ microspheres is formed on a substrate of silicon. In a vacuum environment, ∼2 µm of TiO$_2$ is deposited at an oblique angle of 85° while steadily rotating the substrate about the surface normal. After deposition, the substrate is annealed at 500 °C for 2 hours. An alloy of Au/Pd is then sputtered onto the annealed sample. (b) The top–left panel shows a scanning electron microscope image, while the other images are elemental maps obtained by EDS. (c) The plot shows the ratio of the counts from EDS of the metal alloy to the sum of the counts for the alloy and titanium *vs.* the reported thickness. Inset: A video frame showing a single active particle in water, just above the interface between the liquid and solid.

elongated segment of TiO$_2$, as shown in Fig. 1. A schematic of the fabrication steps—ordered from top-to-bottom—is given in Fig. 1a. We begin with a monolayer of SiO$_2$ microspheres (Bangs Laboratories, Fishers, IN) of ∼3.2 µm in diameter and deposit ∼2 µm of TiO$_2$ at an oblique angle[23] of ∼85° in a vacuum environment (∼10^{-6} Torr) using electron-beam deposition. While the material deposits onto the monolayer, the substrate is rotated about an axis parallel to the surface normal. After deposition, the entire substrate is annealed to 500 °C for about 2 hours,[12] in order to convert the TiO$_2$ to primarily the anatase phase. An alloy made from gold and palladium (Au : Pd = 60 : 40, Denton Vacuum, Moorestown, NJ) is subsequently sputtered atop the substrate, but to different thicknesses, controlled by altering the amount of time the sputtering process lasts—the thickness *vs.* time has been calibrated on-site. Note that Au/Pd alloys have been shown to be more catalytically active than either metal alone in certain cases, *e.g.* for the production of hydrogen.[24,25] We utilized energy-dispersive X-ray spectroscopy (EDS) in order generate the elemental maps shown in Fig. 1b (for the reported (nominal) thickness = 40 nm case), and compare these maps with the scanning electron microscope (SEM) image in the top-left panel of Fig. 1b. Note that the metal alloy tends to cover primarily the "top" TiO$_2$-segments of the Janus particles, as expected. We furthermore obtain the ratio of elemental titanium (Ti) to Au plus Pd, which is given in Fig. 1c for six different thicknesses of the alloy. Each sample originated from the same batch deposition for the TiO$_2$/SiO$_2$ underpinning (top three steps in Fig. 1a). Thus, the relative quantity of the alloy elements to Ti—measured as counts by EDS—should give an accurate representation of how the amount of alloy changes for each sample (Fig. 1c).

After fabrication, the particles are removed from the surface and suspended in de-ionized water by brief bath-sonication. A droplet of the colloid is pipetted onto a clean glass cover-slip, which is subsequently illuminated with UV-light from the bottom (see Fig. 2a) by means of an inverted epifluorescence microscope (Nikon Eclipse Ti2). Under these conditions, the particles that
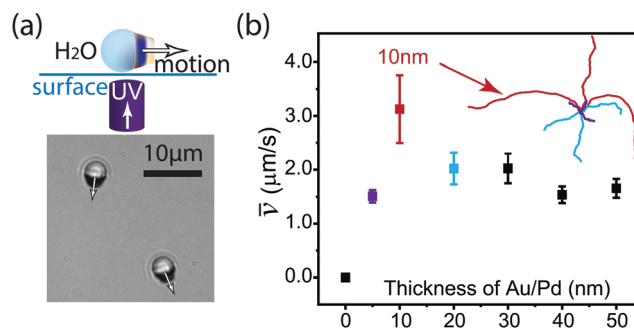
Fig. 2 (a) Schematic of the basic experimental setup: ultraviolet light illuminates the sample from the bottom through a glass cover-slip. The active particles move just above this surface in water alone toward the catalytic portion of the particles, as indicated by the arrows overlaid upon the video frame. (b) Quantitative results showing the relationship between the reported thickness of the Au/Pd alloy and the average speed, $\bar{v}$, calculated from the speeds of fifty individual particles for each thickness. The highest average speed, measured for a thickness of 10 nm, is labeled directly in the plot. Inset: Example trajectories over a ∼10 s time period for the 5 nm, 10 nm, and 20 nm cases, which are color-coded to match the data points in the main plot.

have any amount of the Au/Pd alloy—with the exception of alloy thickness = 0 nm—begin to self-propel away from the SiO$_2$ side (Fig. 2a), sliding just above the glass slip.

The goal of our experiment is to quantify how the amount of the Au/Pd alloy affects the activity of the particles, which we quantify by measuring the average speed, $\bar{v} = \frac{1}{N}\sum_{n=1}^{N} v_i$, as a function of alloy-thickness. The averages are obtained from the speeds, v_i, of fifty individual particles ($N = 50$) for each reported thickness; these data are shown in Fig. 2b. Note that we find no active propulsion if the alloy is absent: $\bar{v} = 0$ if the reported thickness = 0 nm, but non-zero activity is observed for all other thickness of Au/Pd. In order to determine v_i, we track the two-dimensional trajectories, *i.e.* the particles are confined to move above the glass slide *via* gravity (see bottom of Fig. 2b),

at a frame rate of 15 fps. Example trajectories for three different thicknesses, 5 nm, 10 m, and 20 nm, are shown in the inset of Fig. 2b. Next, we determine the mean-squared displacement, $\mathrm{MSD} \simeq \bar{v}^2(\delta t)^2 + 4D\delta t$, where D is the diffusion coefficient. This equation is an approximation for the MSD for delay-times, δt, that are much shorter than the rotational relaxation time, $\tau_r \sim 200$ s. In practice, we fit the MSD-curves for $0 \leq \delta t \leq 3$ s.

To be clear about what is measured in Fig. 2b, we maintain identical experimental parameters, *e.g.* intensity of excitation light, to obtain $\bar{v}$ for each reported thickness of Au/Pd (Fig. 2b). As each sample originates from the same batch fabrication of TiO$_2$/SiO$_2$ Janus particles, the only parameter changing between trials is the thickness of Au/Pd deposited onto the Janus particles (bottom step in Fig. 1a). The fastest average speed is found to occur for the 10 nm-case, which we clearly distinguish in the plot, and the red-arrow points to an example trajectory for this sample. We next qualitatively expand upon the possible reasons for these observations.

We start by reviewing the mechanism of a similar, yet distinct system of fuel-free active colloid: TiO$_2$/Au Janus spheres, which consist of two equal-area faces of each material, are expected to self-propel *via* self-electrophoresis—although other mechanisms could be at play—resulting from water-splitting.[16] When a photon-induced electron–hole pair is generated, $\mathrm{TiO_2} \xrightarrow{h\nu} \mathrm{e^-} + \mathrm{h^+}$, the electrons are attracted to the Au due to a contact potential between the metal and semiconductor. Protons are generated on the TiO$_2$ side by water oxidation

$$2\mathrm{H_2O} + 4\mathrm{h^+} \rightarrow \mathrm{O_2} + 4\mathrm{H^+}, \qquad (2)$$
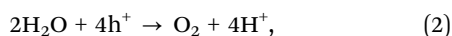
which migrate in the solution to the metal side, where they recombine with the electrons,

$$4\mathrm{H^+} + 4\mathrm{e^-} \rightarrow 2\mathrm{H_2}, \qquad (3)$$
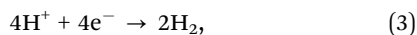
which is the reduction reaction. The motion of the protons results in a flow over the surface the particle, which consequently moves in the direction opposite to this flow, *i.e.* movement is observed toward the TiO$_2$ face. The currently considered system, despite having some similarities to the TiO$_2$/Au Janus sphere, is different due primarily to the manner in which the Au/Pd co-catalyst is distributed upon the TiO$_2$. We would like to explore why any particular combination of Au/Pd and TiO$_2$, for the specific morphology considered herein, should give rise to the highest average speed. We argue this effect is likely due to optimizing the efficiency of the water-splitting process (eqn (2) and (3)), to where we now shift our focus.

Thin films of vapor-deposited Au tend to form nanoscale, three-dimensional nano-islands for thicknesses <15 nm;[26] thicker amounts of Au result in continuous thin films.[27] The geometry of our particular system differs from the two cited studies, which investigate how the Au attaches to flat TiO$_2$. Nevertheless, the highest average speed we observe is the 10 nm-case (see Fig. 2b), which falls within the range of a discontinuous film of the alloy—assuming the Au/Pd thin-films behave approximately the same as pure Au films. We also note that for particles like those herein, as verified from SEM images (see Fig. 1b), the coverage of the TiO$_2$ is expected to be less than what would otherwise be observed for metal deposition onto a flat TiO$_2$ surface. Thus, the most active particles observed herein should likewise consist of Au/Pd islands attached to the TiO$_2$ segments, with areas of the oxide exposed to the solution. We were unable to image directly the distribution of the metal catalyst upon the TiO$_2$ segments. However, in the ESI,† we have provided transmission electron microscope images, which appear to show the presence of such nano-islands. We next explore a possible connection between a partial coverage of the co-catalyst and the photocatalytic efficiency.

The improved photocatalytic performance of TiO$_2$ with the addition of a co-catalyst like Au, which results from the suppression of electron–hole recombination,[28] depends upon the specific morphology of the multi-catalyst material. We turn to the literature and find instances in which partial coverage of a co-catalyst leads to improved efficiency: the breakdown of methyl orange was shown to increase by >100% by optimizing the coverage of Au on TiO$_2$,[29] while the maximal degradation rate of methylene blue was observed to occur for a thickness of ~ 15 nm,[30] to name only a couple. For the latter study, the authors attribute the reduced efficiency with co-catalyst thickness >15 nm to a few different factors including a decrease in surface area for the photocatalytic activity as well as increased light-absorbance from the Au layer. In passing, we mention that the measurement of speed of active particles (Fig. 2b) moving *via* the water-splitting self-electrophoresis mechanism could serve as a means of quantifying catalytic efficiency, complementing typical measurements such as the breakdown of organic dyes.

Thus, a likely reason for the observed highest average speed reported in Fig. 2b results from this morphology maximizing the water-splitting process, by balancing two competing effects: (1) enhanced water-splitting efficiency is provided by the presence of the Au/Pd alloy, and (2) the reduction in efficiency that arises due to the alloy shielding the TiO$_2$ from the solution and the activating light source. In short, a simple enhancement of the catalytic activity appears to be the foundation for the observed effects. We note that the partial coverage of a single catalyst upon a non-catalytic particle, *e.g.* silica/platinum Janus spheres moving in hydrogen peroxide, would, on the contrary, reduce the catalytic efficiency.[31] However, up to a four-fold increase in speed has been observed in such particles by increasing the surface roughness of the platinum catalyst,[32] but in this case the metal remains continuous.

To summarize, tuning the material properties of active colloids can improve the efficiency of fuel-free self-propulsion in water alone. We have demonstrated this effect by observing the average speed of light-activated TiO$_2$-based colloids with differing amounts of an Au/Pd alloy, which serves as a co-catalyst. We find that the maximal average speed, taken from an ensemble of fifty particles for each thickness considered, occurs at an ''intermediate'' thickness—in this case 10 nm of the alloy. Based upon numerous reports from the literature, a thickness around this amount result in metallic nano-islands as opposed to a continuous thin-film. Such a morphology is expected to improve the catalytic efficiency. Thus, a general starting point for constructing efficient fuel-free active colloids of this variety is to deposit a thin film with a

thickness in the range of 10–15 nm. This way there will be sufficient co-catalyst to allow fuel-free motion to take place, without hindering the action of the composite catalyst.

Conflicts of interest

There are no conflicts to declare.

References

1 G. Zhao, B. Khezri, S. Sanchez, O. G. Schmidt, R. D. Webster and M. Pumera, *Chem. Commun.*, 2013, **49**, 9125–9127.
2 J. Gibbs and P. Fischer, *Chem. Commun.*, 2015, **51**, 4192–4195.
3 Y. Gu, S. Sattayasamitsathit, K. Kaufmann, R. Vazquez-Duhalt, W. Gao, C. Wang and J. Wang, *Chem. Commun.*, 2013, **49**, 7307–7309.
4 S. Sánchez, L. Soler and J. Katuri, *Angew. Chem., Int. Ed.*, 2015, **54**, 1414–1444.
5 T. Yu, P. Chuphal, S. Thakur, S. Y. Reigh, D. P. Singh and P. Fischer, *Chem. Commun.*, 2018, **54**, 11933–11936.
6 U. Choudhury, A. V. Straube, P. Fischer, J. G. Gibbs and F. Höfling, *New J. Phys.*, 2017, **19**, 125010.
7 F. Ginot, A. Solon, Y. Kafri, C. Ybert, J. Tailleur and C. Cottin-Bizonne, *New J. Phys.*, 2018, **20**, 115001.
8 J. N. Johnson, A. Nourhani, R. Peralta, C. McDonald, B. Thiesing, C. J. Mann, P. E. Lammert and J. G. Gibbs, *Phys. Rev. E*, 2017, **95** 042609.
9 A. Nourhani, S. J. Ebbens, J. G. Gibbs and P. E. Lammert, *Phys. Rev. E*, 2016, **94**, 030601.
10 S. Sanchez, A. A. Solovev, S. Schulze and O. G. Schmidt, *Chem. Commun.*, 2011, **47**, 698–700.
11 S. Ramananarivo, E. Ducrot and J. Palacci, *Nat. Commun.*, 2019, **10**, 1–8.
12 D. Nicholls, A. DeVerse, R. Esplin, J. Castaneda, Y. Loyd, R. Nair, R. Voinescu, C. Zhou, W. Wang and J. G. Gibbs, *ACS Appl. Mater. Interfaces*, 2018, **10**, 18050–18056.
13 J. G. Gibbs, *Langmuir*, 2019, DOI: 10.1021/acs.langmuir9b02866.
14 K. Villa, F. Novotný, J. Zelenka, M. P. Browne, T. Ruml and M. Pumera, *ACS Nano*, 2019, **13**, 8135–8145.
15 D. P. Singh, U. Choudhury, P. Fischer and A. G. Mark, *Adv. Mater.*, 2017, **29**, 1701328.
16 R. Dong, Q. Zhang, W. Gao, A. Pei and B. Ren, *ACS Nano*, 2015, **10**, 839–844.
17 J. G. Gibbs, S. Sarkar, A. Leeth Holterhoff, M. Li, J. Castañeda and J. Toller, *Adv. Mater. Interfaces*, 2019, **6**, 1801894.
18 K. Maeda and K. Domen, *J. Phys. Chem. Lett.*, 2010, **1**, 2655–2661.
19 M. Ni, M. K. Leung, D. Y. Leung and K. Sumathy, *Renewable Sustainable Energy Rev.*, 2007, **11**, 401–425.
20 M. Ibele, T. E. Mallouk and A. Sen, *Angew. Chem., Int. Ed.*, 2009, **48**, 3308–3312.
21 É. O'Neel-Judy, D. Nicholls, J. Castañeda and J. G. Gibbs, *Small*, 2018, **14**, 1801860.
22 N. Alenzi, W.-S. Liao, P. S. Cremer, V. Sanchez-Torres, T. K. Wood, C. Ehlig-Economides and Z. Cheng, *Int. J. Hydrogen Energy*, 2010, **35**, 11768–11775.
23 H.-H. Jeong, A. G. Mark, J. G. Gibbs, T. Reindl, U. Waizmann, J. Weis and P. Fischer, *Nanotechnology*, 2014, **25**, 235302.
24 R. Su, R. Tiruvalam, A. J. Logsdail, Q. He, C. A. Downing, M. T. Jensen, N. Dimitratos, L. Kesavan, P. P. Wells and R. Bechstein, *et al.*, *ACS Nano*, 2014, **8**, 3490–3497.
25 M. Bowker, C. Morton, J. Kennedy, H. Bahruji, J. Greves, W. Jones, P. R. Davies, C. Brookes, P. Wells and N. Dimitratos, *J. Catal.*, 2014, **310**, 10–15.
26 A. Kossoy, D. Simakov, S. Olafsson and K. Leosson, *Thin Solid Films*, 2013, **536**, 50–53.
27 L. Zhang, F. Cosandey, R. Persaud and T. E. Madey, *Surf. Sci.*, 1999, **439**, 73–85.
28 V. Subramanian, E. Wolf and P. V. Kamat, *J. Phys. Chem. B*, 2001, **105**, 11439–11446.
29 I. Arabatzis, T. Stergiopoulos, D. Andreeva, S. Kitova, S. Neophytides and P. Falaras, *J. Catal.*, 2003, **220**, 127–135.
30 D. Zhou, Y. Liu, W. Zhang, W. Liang and F. Yang, *Thin Solid Films*, 2017, **636**, 490–498.
31 S. Ebbens, D. Gregory, G. Dunderdale, J. Howse, Y. Ibrahim, T. Liverpool and R. Golestanian, *Europhys. Lett.*, 2014, **106**, 58003.
32 U. Choudhury, L. Soler, J. G. Gibbs, S. Sanchez and P. Fischer, *Chem. Commun.*, 2015, **51**, 8660–8663.